Journal of Sol-Gel Science and Technology (2021) 99:158–168
https://doi.org/10.1007/s10971-021-05559-1

ORIGINAL PAPER: NANO-STRUCTURED MATERIALS (PARTICLES, FIBERS, COLLOIDS, COMPOSITES, ETC.)

Synthesis of novel $ZnAl_2O_4/Al_2O_3$ nanocomposite by sol–gel method and its application as adsorbent

A. Saffar[1] · H. Abbastabar Ahangar[1] · Shahriyar Salehi[2] · M. H. Fekri[3] · A. Rabbani[1]

Received: 24 January 2021 / Accepted: 20 May 2021 / Published online: 18 June 2021

Abstract

In this research, $ZnAl_2O_4/Al_2O_3$ nanocomposites with different $ZnAl_2O_4$ (30, 50, and 70 wt.%) were successfully prepared in one step by sol–gel method and utilized for the removal of methylene blue (MB). The structural properties of nanocomposites were investigated by X-ray diffraction (XRD), differential thermal analysis (DTA), FTIR analysis, Zeta potential, and BET. The obtained results showed the synthesized nanocomposites by sol–gel method were amorphous and heat treatment at 700 °C led to the crystallization of zinc aluminate spinel. The maximum MB removal (70%) was obtained under o9 ptimal conditions such as initial concentration of MB (10 mg/L), pH of solution (8.5), the amount of adsorbent (0.05 g), type of adsorbent (70 wt.% $ZnAl_2O_4/Al_2O_3$ nanocomposite). The average size of zinc aluminate crystals in the maximum amount of zinc aluminate in the composite (70 wt.%) was calculated to be 27 ± 1 nm and its morphology changed from sheet to mass. The specific surface area of the nanocomposite was calculated to be 70 m^2/g. The kinetics of adsorption was fitted with the pseudo-second order model.

Graphical Abstract

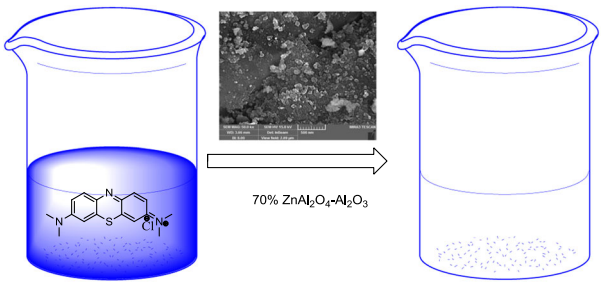

Keywords Nanocomposite · Al_2O_3–$ZnAl_2O_4$ · Sol–gel · Spinel · Adsorbent.

Highlights

- $ZnAl_2O_4/Al_2O_3$ nanocomposites with different $ZnAl_2O_4$ were synthesized in one step by sol–gel method.
- The specific surface area of Al_2O_3 –70 wt.% $ZnAl_2O_4$ nanocomposite was calculated to be 70 m^2/g.
- The highest adsorption efficiency MB (72%) was obtained from 10 mg/L initial solution.

✉ A. Saffar
a.saffar.t@iaun.ac.ir

[1] Department of Chemistry, Najafabad Branch, Islamic Azad University, Najafabad, Iran

[2] Advanced Materials Research Center, Department of Materials Engineering, Najafabad Branch, Islamic Azad University, Najafabad, Iran

[3] Department of Chemistry, Ayatollah Borujerdi University, Borujerd, Iran

1 Introduction

Oxide spinels include a large group that are technologically and geologically important. Spinels containing iron and zinc are technologically important due to their magnetic properties and insulation [1–3]. Zinc aluminate with a spinel structure is a semiconductor with a band gap about 3.8 eV and indicates these systems are electrically conductive and transparent at wavelengths above 320 nm [4]. It is widely used in many applications due to optical properties, high chemical and physical stability, high mechanical strength and low surface acidity [5, 6]. In addition, $ZnAl_2O_4$ ultrafiltration membranes were used for removing the heavy metals and carmoisine (colorant) from wastewater [7]. Therefore, $ZnA1_2O_4$ with respect to the selection of sorbent has a good potential to optimize aquatic environmental remediation technologies.

Tzing and Tuan [2] reported the preparation he duplexes $A1_2O_3$–$ZnA1_2O_4$ by reaction sintering of alumina and zinc oxide at 1650 °C with high resistance to coarsening at an elevated temperature. Zhaoxia et al. [8] synthesized $ZnAl_2O_4$/α-Al_2O_3 using the solid-phase reaction of pulsed-laser-deposited ZnO film and α-Al_2O_3 substrate with transformation from uniform islands to stick structures. Sukul and Balaramakrishna [1] reported an in-situ sol–gel route for preparation of nanocrytalline $ZnAl_2O_4$ dispersed in silica matrix. From the XRD results, the crystalline $ZnAl_2O_4$ phase was formed for samples heat treated at different temperatures in the range of 800 to 1200 °C. Zhang et al. [3] prepared spheres-in-spheres ZnO/$ZnAl_2O_4$ composite hollow microspheres by hydrothermal method with the highest specific surface area and no particle agglomeration at 25 mol% ZnO. In addition, $ZnAl_2O_4$ nanocatalyst has the ability to remove dyes from contaminated water under sunlight [9]. So far, $ZnAl_2O_4$ nanocrystals have been synthesized by different methods such as co-precipitation, hydrothermal, microwave, combustion Technique [10], sol–gel [6], and soluble phase method [11]. Among the available methods, sol–gel method is a cost-effective and simple method with chemical homogeneity, very uniform fuzzy distribution, for multi-component systems, and the possibility of preparing new crystalline and non-crystalline materials [12, 13].

Gamma-alumina is one of the most widely used support which is a phase with an incomplete spinel structure and a large surface area. It is converted to hexagonal alpha-alumina at 900 °C [14].

In the last decade, the rapid industrialization led to global climate change, reduction of water reserves, and increasing contamination of water resources. The synthetic dyes are the most hazardous pollutant for human and aquatic life because of their chemical and physical properties. Adsorption is one of the most attractive techniques for wastewater treatment due to its low cost, simplicity and the availability of a wide range of adsorbents. Therefore, the development of synthetic method of $ZnAl_2O_4$ in the presence of silica and alumina was suggested to give new characteristics and further applications.

Based on our studies, no report has been found on the adsorption properties of the two-component $ZnAl_2O_4$/Al_2O_3 nanocomposite. It was confirmed that the coexistence of different crystalline phases led to improve physiochemical properties with higher photocatalytic and adsorption activity. It can be attributed to change morphology, produce unique interfaces between phases, and change zeta potential.

In this paper, the influence of the changing different wt.% of $ZnAl_2O_4$ in $ZnAl_2O_4$/Al_2O_3 nanocomposite on surface charge, morphology, particle size, and specific surface area of the sample is investigated. Then, the kinetics of adsorption was evaluated by using methylene blue dye adsorption.

2 Material and method

2.1 Synthesis of $ZnAl_2O_4$ /Al_2O_3 nanocomposite by sol–gel method

$ZnAl_2O_4$/Al_2O_3 nanocomposite was prepared with different weight percent of $ZnAl_2O_4$ (30, 50, and 70 wt.%). For synthesis of $ZnAl_2O_4$/Al_2O_3 nanocomposite with 30 wt.% $ZnAl_2O_4$, first 5.025 g of aluminum nitrate ($Al(NO_3)_3{\cdot}9H_2O$) was added to 100 ml of deionized water containing 2 g of zinc nitrate ($Zn(NO_3)_2{\cdot}6H_2O$) and then placed at room temperature on a magnetic stirrer at 150 rpm to dissolve completely. To this solution, 81.241 g of citric acid was added and stirred at ambient temperature for 20 min. In the next step, 4.4 g of aluminum hydroxide ($Al(OH)_3$) was added to the obtained solution and the mixture placed on a stirrer at 80 °C for 5 h and the gel was obtained. The resulting gel (xerogel) was placed in an oven for 24 h at 120 °C. Finally, the obtained powder was calcined at 700 °C for 3 h. Samples with 50 and 70 wt.% $ZnAl_2O_4$ were prepared in a similar way.

2.2 Characterization

The crystal structures were studied by X-ray diffractometer (XRD, Philips *X'Pert–PRO*, PW3050/60 diffractometer). Fourier transform infrared spectroscopy was recorded by the JASCO Model FT/IR-6300 spectrometer using KBr as the reference sample within the wavelength range of 400–4000 cm^{-1}. The surface morphology of the nanocomposites was investigated by field-emission scanning electron microscopy (Cam scan MV2300) and transmission electron microscopy (TEM, JEM-100CX, Japan). In order to determine the zeta potential of the samples, a zetasizer

was used by Malvern company of England at 25 °C and dispersed in water with pH = 8.5.

2.3 Adsorption experiments

The dye removal experiments were performed at room temperature by Optizen 3220 UV Spectrophotometer at a wavelength of 665 nm. A stock solution (1000 mg/L) of MB dye was prepared in deionized water, then experimental solutions with different initial concentrations (5–30 mg/L) were obtained by successive dilutions. The required amount of $ZnAl_2O_4$–Al_2O_3 nanocomposite was added into the 10 mL dye solution and stirred for the predefined time. After that, the suspension was centrifuged and the supernatant was analyzed by ultraviolet–visible light (UV–Vis) spectroscopy to calculate the residual dye concentration. The removal of dye percentage (R) was measured using the following equation:

$$R\% = ((C_0 - C_t)/C_0) \times 100 \quad (1)$$

where C_0 is the initial concentration and C_t is the concentration of the dye at time t [15, 16].

2.4 Adsorption kinetics

To study the adsorption mechanism, the dye adsorption constants can be measured by the pseudo-first-order kinetic equation and the pseudo-second-order kinetics. The adsorption kinetics can be described by pseudo-first-order kinetics:

$$l(q_{eq} - q) = \ln q_{eq} - \frac{K_1 t}{2.303} \quad (2)$$

In this equation, q_{eq} and q are the amount of dye adsorbed at equilibrium and the amount of dye adsorbed at t, respectively, in mg/g and K_1 is the pseudo-first-order adsorption equilibrium constant. A straight line is obtained by plotting log $(q_e - q)$ versus t, which can be used to obtain the K_1 constant and the R^2 correlation coefficient [3].

The adsorption kinetics can also be explained by the pseudo-second-order kinetics model.

$$\frac{t}{q} = \frac{1}{K_2 q_{eq}^2} + \frac{1}{q_{eq}} t \quad (3)$$

So that, q is the amount of dye adsorbed at equilibrium in mg/g and K_2 is the equilibrium rate of the pseudo-second equilibrium rate [3, 15–17]. If the pseudo-quadratic equation is applicable, the graph of t/q versus t from the above equation should show a linear relationship. q and K_2 are determined from the slope and intersection point of the graph, respectively.

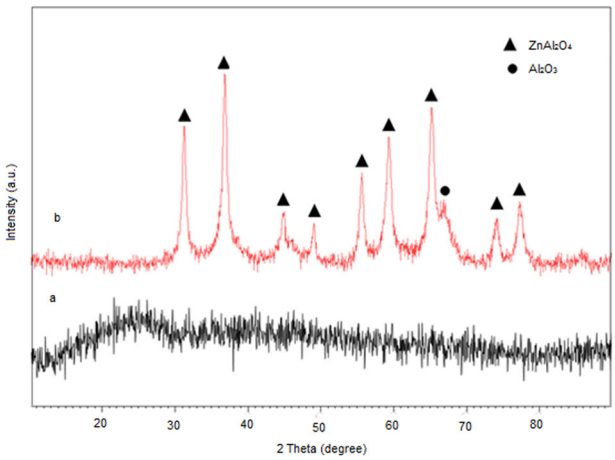

Fig. 1 XRD patterns of 50 wt.% $ZnAl_2O_4$–Al_2O_3 **a** before and **b** after heat treatment at 700 °C

3 Results and discussion

3.1 XRD

All the samples were heat treated at 700 °C for 3 h at a rate of 10 °C/min according to published data [1, 3, 15, 16]. Figure 1 shows the X-ray diffraction pattern of the Al_2O_3–50% $ZnAl_2O_4$ sample before and after heat treatment at 700 °C. No peak diffraction is observed in the synthesized sample as sub-gel, which indicates the amorphous nature of the synthesized product by the sol–gel method [1, 3, 15].

It is clear that in the 100% Al_2O_3 sample, the presence of wide peaks (JCPDS No. 01-088-0826) indicates the lack of high crystallization of Al_2O_3 particles in this sample. The presence of an amorphous phase affects the peak intensity of the crystalline phase. $ZnAl_2O_4$ phase diffraction peaks increased slightly by decreasing the amount of Al_2O_3 in the composite (Fig. 2).

In the 100% $ZnAl_2O_4$ sample, weak peaks of ZnO phase are observed, which are not observed in nanocomposite samples. The reason for this was attributed to the presence of Al_2O_3 phase in the composite, which had a weak crystallization at a temperature of 700 °C. The sharpening of the peaks is due to the increase in crystallinity and the size of the sample crystal [16]. According to the X-ray diffraction pattern of the samples (Fig. 2), certain peaks at 2θ = 31.22, 36.77, 44.69, 48.98, 52.55, 59.27, 65.06, 73.12, and 77.97° are observed, which are related to crystal planes (220), (311), (400), (331), (422), (511), (440), (620) and (533) reflections of the cubic space group Fd3m $ZnAl_2O_4$ spinel structure (JCPDS No. 05-0669).

The Williamson–Hall method was used to calculate the crystal size of $ZnAl_2O_4$ in the composite. The Williamson–Hall

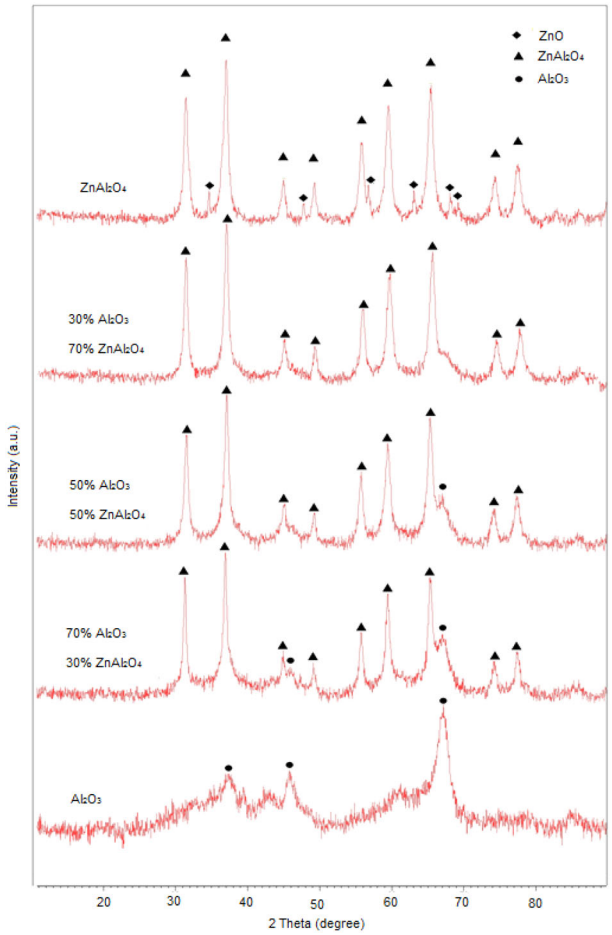

Fig. 2 XRD patterns of different wt.% $ZnAl_2O_4$–Al_2O_3

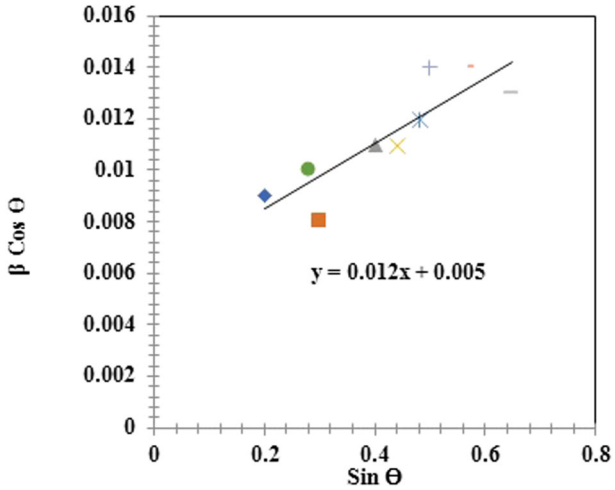

Fig. 3 Estimation of the crystallite size and strain of 70 wt.% $ZnAl_2O_4$–Al_2O3 nanocomposite from the X-ray diffraction data using the Williamson–Hall method

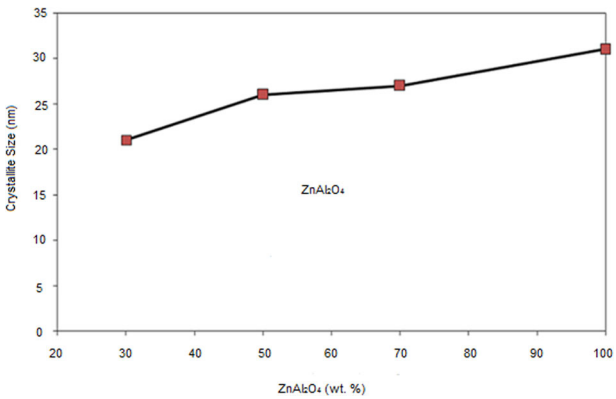

Fig. 4 The effect of wt.% $ZnAl_2O_4$ on the crystal size of $ZnAl_2O_4$–Al_2O_3

relationship is as follows [16]:

$$\beta \cos\theta = \frac{0.9\lambda}{D} + 2A\varepsilon \sin\theta \tag{4}$$

where λ wavelength is usually a copper lamp 0.154 nm, D crystal size, A is constant, ε strain, β peak width at half maxima and θ is the Bragg angle. Zigma Plot software was used to increase the accuracy and eliminate errors in measuring the width of the peaks. Figure 3 shows the Williamson–Hall diagram of the 70 wt.% $ZnAl_2O_4/Al_2O_3$ composite.

As the percentage of $ZnAl_2O_4$ in the composite structure increases, the peaks of the zinc aluminate phase have increased indicating the growth and enlargement of $ZnAl_2O_4$ crystals in $ZnAl_2O_4$–Al_2O_3 nanocomposites (Fig. 4).

3.2 Identify the types of bonds and investigate the effect of temperature on the type of bonds

In the spectrum of the xerogel sample, the presence of absorption bands at 3526 cm^{-1} and 3463 cm^{-1} is related to the presence of metal hydroxyl groups, which their absorption intensity has been reduced due to heat treatment at 700 °C [1, 3]. The absorption bands from 1203 to 1403 cm^{-1} in the xerogel spectrum confirm the presence of nitrate groups (aluminum nitrate and zinc nitrate). The bending and stretching vibrations of the O–H group of water molecules were observed at 1624 and 1722 cm^{-1}, respectively [3, 16, 18]. Figure 5 shows the absorption band at 670 cm^{-1} in the sub-gel spectrum related to zinc spinel aluminate, which has intensified after heat treatment. Three absorption bands were appeared at 672, 550, 509 cm^{-1} related to Al–O stretching vibrations, O–Al–O bending vibrations in octahedral structure of the AlO_6 group, and the stretching vibrations of the Zn–O in the tetrahedral spinel group, respectively. The 1641 cm^{-1} band in the heat treatment sample is related to H–O–H flexural vibrations [19]. Also, the presence absorption band 1383 cm^{-1} in the heat treatment sample refers to the alkoxide groups present in the nanocomposite. By comparing the two FTIR spectra, it is

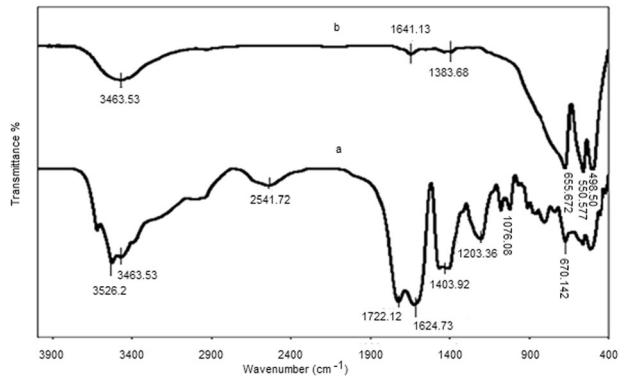

Fig. 5 FTIR spectra of 50 wt.% $ZnAl_2O_4$–Al_2O_3 a. before and b. after heat treatment at 700 °C

found that heat treatment weakens the metal hydroxyl bonds and strengthens the spinel bonds.

3.3 Morphology of Al_2O_3–$ZnAl_2O_4$ nanocomposites ($ZnAl_2O_4$ free)

Figure 6 shows the SEM image and the linear analysis of EDS of Al_2O_3–$ZnAl_2O_4$ nanocomposites after heat treatment at 700 °C. The presence of fine particles in the agglomerated structure $Al(OH)_3$ indicating the lack of high crystallization of the constituent particles after heat treatment confirmed by the wide peaks the XRD results. A bond between aluminum and oxygen was formed after heat treatment at a temperature of 700 °C but not enough driving force for the growth of Al_2O_3. The crystallization of $ZnAl_2O_4$ crystals was observed according to the comparison the morphology of Al_2O_3 particles heat treatment. The fine particles among the larger particles were attributed to the presence of ZnO in the structure of $ZnAl_2O_4$ supported XRD results. According to EDS linear analysis of the sample surface, the presence of three elements Al, Zn, and O in the sample structure is confirmed.

30 wt.% $ZnAl_2O_4/Al_2O_3$ nanocomposite background is low in crystallinity because of the presence of Al_2O_3 phase. The morphology of the nanocomposite is platelet. A linear analysis of the surface of the nanocomposite shows the weight percentage of Zn less than Al and O due to the higher amount of Al_2O_3 phase in the nanocomposite. It is clear that the morphology of $ZnAl_2O_4$–Al_2O_3 nanocomposite has progressed from platelet to aggregate with increasing wt.% of $ZnAl_2O_4$. Particles on the surface of the nanocomposite with an average size of 25 nm are observed, which is close to the calculated crystal size by the Williamson–Hall method (27 nm). The weight percentage of Zn increased significantly in 70 wt.% $ZnAl_2O_4$–Al_2O_3 nanocomposite compared to the 30% $ZnAl_2O_4$–Al_2O_3 nanocomposite.

3.4 Surface area measurement

Adsorption is usually expressed in isotherms that are equivalent to the amount of adsorbent on the surface, which is a function of the amount of pressure (in the case of gases) or the concentration (in the case of liquids) of the adsorbent at constant temperature. Conversely, desorption isotherm is obtained by measuring the amount of desorbed gas. To investigate the change of surface properties, a Al_2O_3–70 wt. % $ZnAl_2O_4$ sample was heat treated at 700 °C and BET test was taken. Figure 7 shows the isotherm diagram of the adsorption and desorption isotherm (77 K) of Al_2O_3–70 wt. % $ZnAl_2O_4$ nanocomposite. When nitrogen is observed in ring adsorption and desorption diagrams, it indicates that this type of isotherm is used for porous materials. When the p/p_0 ratio is large, the material has very narrowed, capillary pores, in which the adsorption rate increases significantly and the adsorbed material condenses on the surface. The synthesized nanocomposite isotherm is a type IV isotherm with a residual ring which shows the mesoporous nature of the cavities [19]. The distance between the absorption and desorption diagrams indicates the existence of porosities in the adsorbent. The specific surface area measured for Al_2O_3–70 wt.% $ZnAl_2O_4$ nanocomposite was 70 $m^2\,g^{-1}$.

The pore size distribution for Al_2O_3–70 wt.% $ZnAl_2O_4$ nanocomposite in both adsorption and desorption modes using BJH theory is shown in Fig. 7. As can be seen, the largest porosity size in the adsorption and desorption state is about 19 nm. The amount of volume and diameter at the peak of the maximum porosity diameters in adsorption was measured as 0.2009 $cm^3\,g^{-1}$ and 2.1 nm, and in desorption were equaled to 0.193 $cm^3\,g^{-1}$ and 1.6 nm, respectively.

3.5 Investigate the color adsorption process

Dyes are one of the most dangerous groups of chemical compounds found in industrial effluents that have considerable importance in light permeability reduction and subsequent disruption of the process of photosynthesis in water sources [20, 21]. The most efficient way to remove organic dyes from industrial effluents is the adsorption process, because the dye compounds in the wastewater are easily transferred to the solid phase. On the other hand, the used adsorbent can be regenerated and reused in the adsorption process or stored in a dry place without direct contact with the environment [21].

First methyl orange dye (as a model of anionic dyes) was used to study the adsorption of synthesized nanocomposites for dye adsorption. Adsorption experiments were performed for this dye but no adsorption was done from methyl orange due to the repulsive force created between the dye and the adsorbent. Therefore, methylene blue as a cationic dye was used to perform the dye adsorption test. In this study,

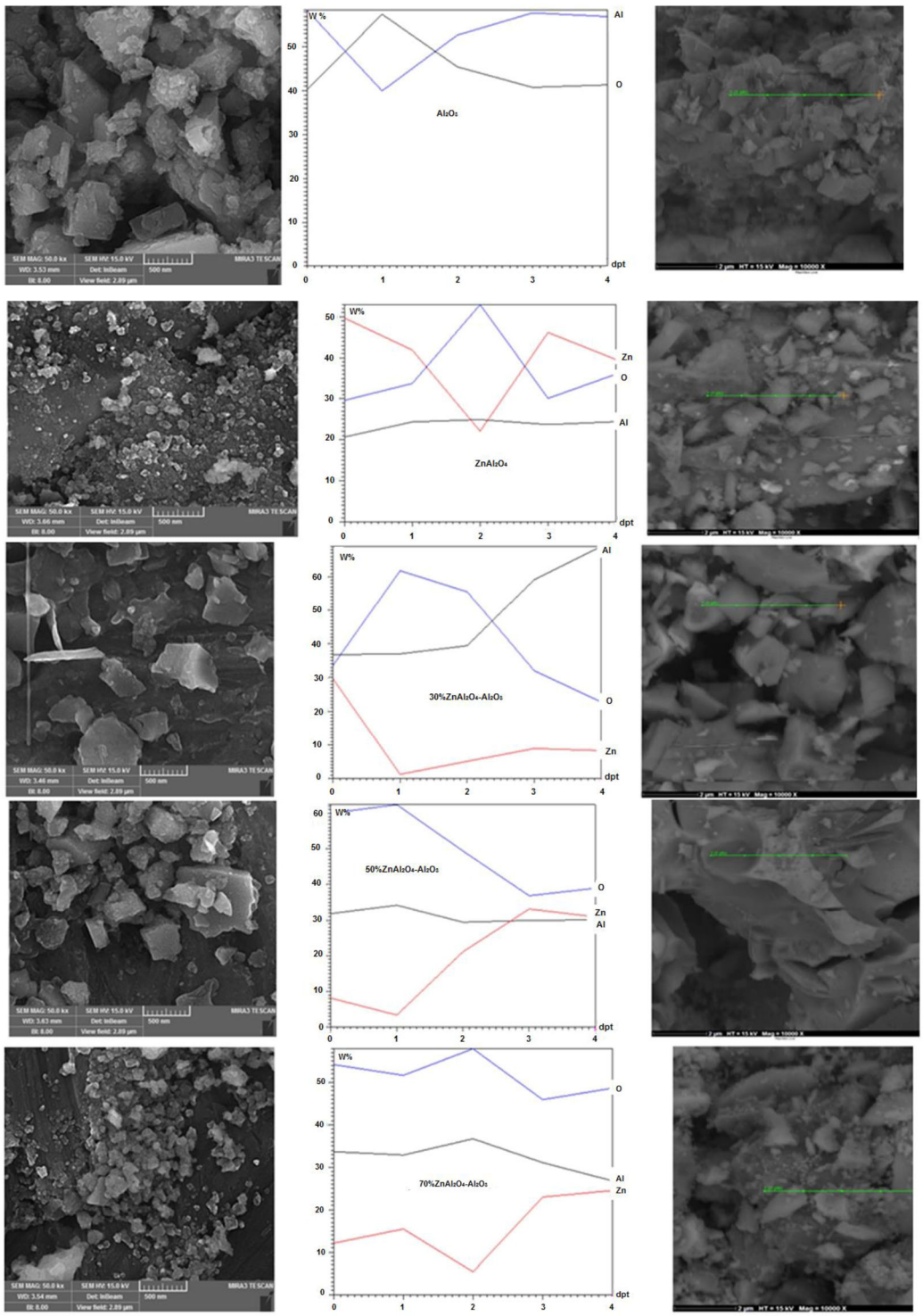

Fig. 6 SEM images and the linear analysis of EDS of $ZnAl_2O_4$–Al_2O_3 nanocomposits

various variables such as contact time, adsorbent amount, and percentage of adsorbent in the sample and initial concentration of methylene blue dye as well as data obtained from equilibrium studies using pseudo-first order and pseudo-second order kinetic models were investigated.

3.6 The effect of adsorbent type on the adsorption efficiency of methylene blue

The effect of $ZnAl_2O_4$ percentage in Al_2O_3–$ZnAl_2O_4$ nanocomposite was investigated on the adsorption process to

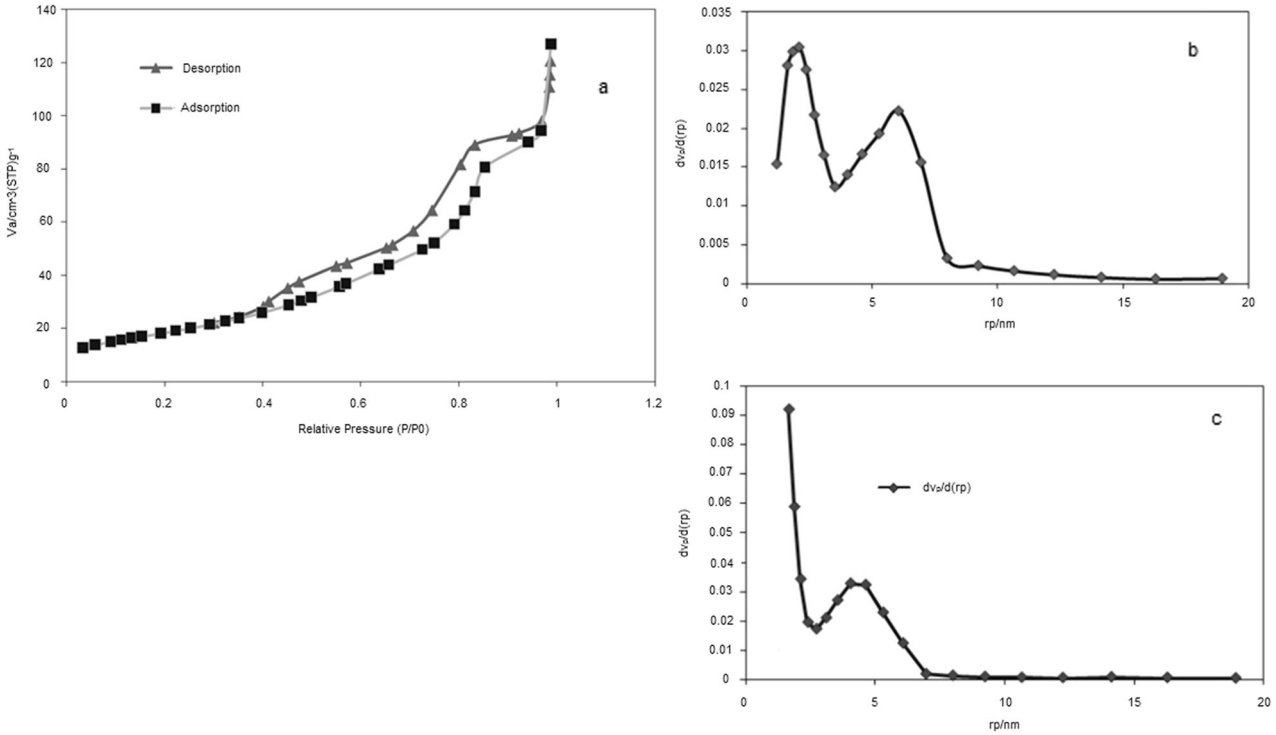

Fig. 7 **a** Nitrogen adsorption–desorption isotherms 70% $ZnAl_2O_4$–Al_2O_3 and pore size distributions **b** adsorption **c** desorption (BJH theory)

obtain the best sample with the highest adsorption efficiency. It should be mentioned that adsorption tests (by default) were performed at pH = 8.5, contact time of 30 min, dye concentration of 10 mg/L, and adsorbent amount of 0.05 g after determination of the residual dye concentration spectrophotometry. The results showed that the highest and lowest percentages of dye adsorption belong to Al_2O_3–70 wt.% $ZnAl_2O_4$ and 100% Al_2O_3, respectively (Fig. 8a).

3.7 Investigation of the effect of adsorbent on methylene blue dye adsorption

The amount of adsorbent used in the adsorption process is one of the most important characteristics of adsorption systems due to the high cost of adsorbent supply in large commercial systems. The amount of adsorbent used to remove various contaminants often depends on the adsorbent properties such as specific surface area, pore size, and total pore volume. With increasing the adsorbent amount from 0.01 g to 0.05 g, the adsorption efficiency has increased 63% (Fig. 8b). The basis of this fact can be interpreted that by increasing the amount of adsorbent under equal conditions, active and available places for interactions between the adsorbates and the adsorbent component (methylene blue dye) of the solution increase and in this regard the adsorption capacity increases with increasing the amount of adsorbent.

3.8 Investigation of the effect of initial concentration of methylene blue dye on the adsorption process

The initial concentration of the dye provides a considerable driving force to overcome the total resistance resulting from the transfer of dye mass between the liquid and solid phases [22]. Figure 8c shows the effect of the initial concentration of methylene blue dye on the adsorption by the nanocomposite. The highest absorption of methylene blue is observed at a concentration of 10 mg/L.

Increasing the concentration of the primary dye reduces the adsorption efficiency. It can be attributed to the molecules of the dye are rapidly adsorbed on the adsorbent surface at low concentrations of the dye, and by increasing the initial concentration of the dye leads to saturation of the adsorbent surface in a short time or electrostatic repulsion between the cationic dye molecules, thus reducing the amount of adsorption [23, 24].

In other words, the amount of adsorption not only depends on to electrostatic interactions between the dye and the adsorbent, but also the ratio of the number of moles of dye to the active sites on the adsorbent surface [25]. The ratio of the initial number of moles of methylene blue to the active sites increases, resulting in a decrease in the percentage of dye adsorption [26], so to continue experiments, the optimal concentration of methylene blue is 10 mg/L.

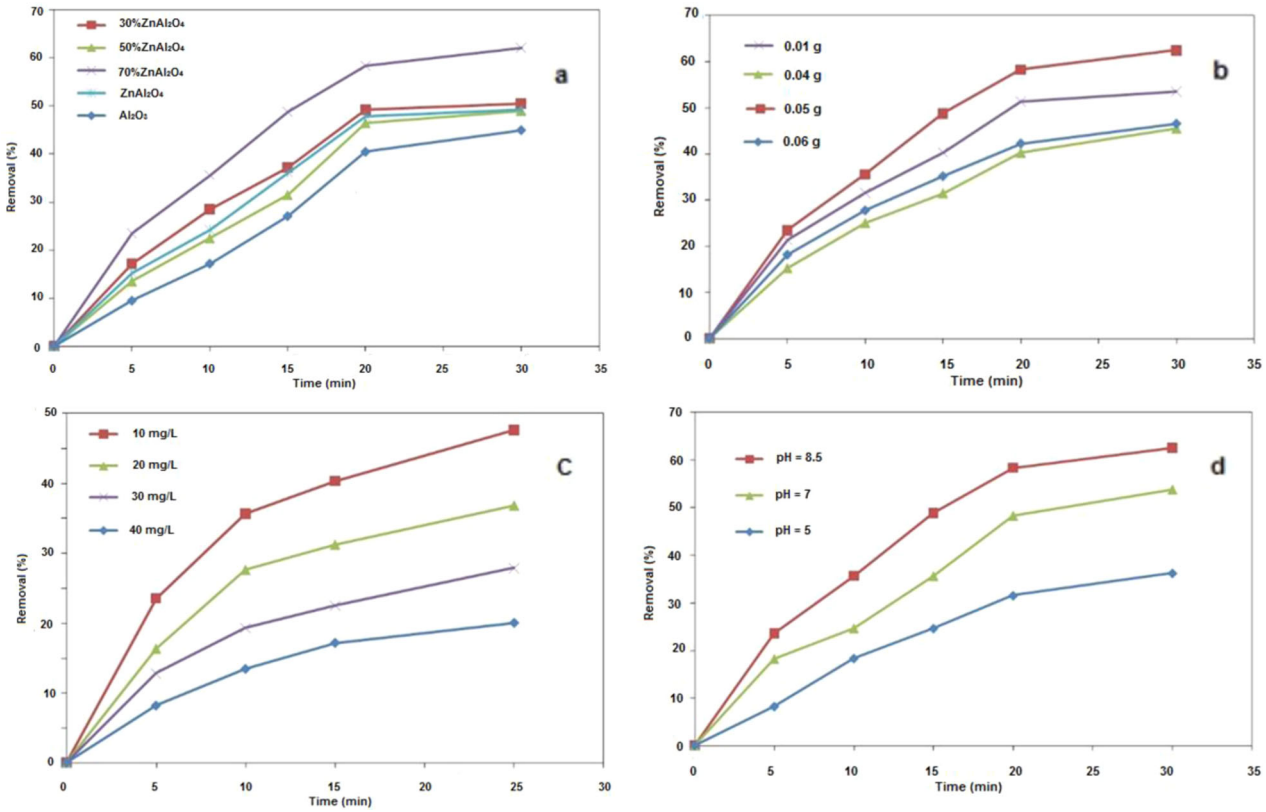

Fig. 8 Effect of **a** adsorbent type **b** adsorbent dosage **c** initial MB concentration **d** pH on the adsorption of MB by $ZnAl_2O_4$–Al_2O_3 nanocomposite

3.9 Optimization of pH point and its effect on adsorption

pH is one of the important factors that affect the surface properties and the surface charge of the adsorbent in the adsorption process. The pH of the solution affects the chemistry of the aqueous medium and the absorbent surface, and therefore the pH of the solution is an important parameter during the dye adsorption process. It has been reported that the adsorption reaction with cationic dyes is mainly through the interactions between hydrogen bonds and van der Waals forces [27].

To investigate the effect of pH on the absorption of methylene blue dye by Al_2O_3–70 wt.% $ZnAl_2O_4$ nanocomposite heat treated at 700 °C, experiments at different pH values (5, 7 and 8.5) at a concentration of 10 mg/L, the amount of adsorbent 0.05 g and ambient temperature were determined and after 30 min the residual color concentration was determined by spectrophotometry. The results of these experiments are shown in Fig. 8. The results of experiments showed that with changes in pH from 5 to 8.5, the efficiency of the adsorption process increases, so that at pH = 8.5 the highest adsorption efficiency was achieved.

This can be explained by considering the electrostatic interaction between the negative fluxes at a large level of the adsorbent, which leads to the adsorption of the cationic dye methylene blue. In other words, with increasing pH to 8.5, the concentration of OH^- ion in solution is high, it causes the H^+ ion to be removed from the OH groups on the adsorbent, resulting the number of negatively charged sites increases. As the surface of the adsorbents receives more negative charge, the interaction between the adsorbents and the cationic dye molecules also increases [28, 29].

Therefore, the adsorption capacity of adsorbents increases with increasing pH value, and at low pH values of the solution, the high concentration of hydrogen ions causes more positive charge on the adsorbents, which prevents the adsorption of cationic dyes on the adsorbent. Therefore, excess hydrogen ions compete with cationic dye molecules for adsorption on active sites lead to adsorption capacity of adsorbents is greatly reduced at low pH values [30].

To confirm the above results, zeta potential analysis was used to determine the surface charge. Figure 9 shows the zeta potential test results for 70 wt.% $ZnAl_2O_4$–Al_2O_3 nanocomposite. Due to the shape of the nanocomposite, it has a surface charge of −21.6 mV. The number of negative charges increases with increasing pH because the surface charge of the obtained nanocomposite is negative. The electrostatic interaction between the adsorbent and MB increases and its adsorption efficiency increases.

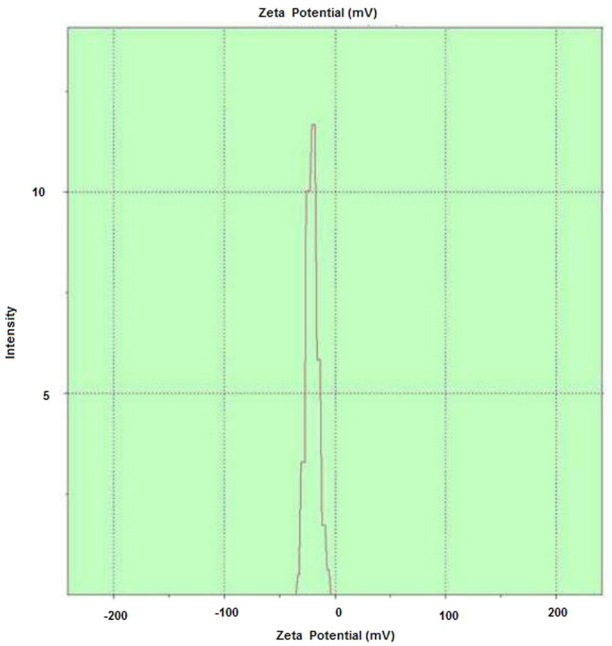

Fig. 9 Zeta potentials graph by $ZnAl_2O_4$–Al_2O_3 nanocomposite at pH = 8.5

Therefore, increasing the absorption can be justified by increasing the pH.

We believed that nanocomposite provides a high specific surface area resulting guarantee their sufficient contact with the dye solution through the reduction of diffusion resistance of the dye molecules.

It might be resulted from the relatively weak chemical reaction between adsorbent and H^+ and OH^- led to the destruction the hydrogen bond in the adsorption process.

When the pollutant solution is exposed to the adsorbent and pulled toward it, attracted and ultimately captured.

Finally, Table 1 shows a comparison of $ZnAl_2O_4$–Al_2O_3 with other works to improve MB dye removal. It can be observed, their physical and chemical characteristics led to the difference removal performance of MB dye. Among the main factors that influence on the adsorption are surface area and initial solution pH.

3.10 Investigation of adsorption kinetic models

One of the most important factors for the design of the adsorption system (to determine the residence time of the adsorbent) is to predict the speed of the adsorption process, which is controlled by the kinetics of the system. Adsorption kinetics depend on the physical and chemical properties of the adsorbent that affect the adsorption mechanism [31]. Adsorption kinetics explain the adsorption rate of methylene blue dye, and this rate controls the equilibrium time. The adsorption kinetics of the adsorbent component are required to select the optimal process conditions on a large scale. Kinetic parameters that are useful for predicting adsorption rate provide important information for process design and modeling. Different models can be used to study the kinetics of the adsorption process, two examples of which are given in this research:

Table 1 Removal of methylene blue by various adsorbents

Adsorbent	Adsorption capcity (mg/g)	pH	Ref
$ZnAl_2O_4$–Al_2O_3	20	8.5	This study
Al_2O_3/SiO_2–50% $CuAl_2O_4$	10	10	[34]
NaOH-treated fly ash	12.8	8	[33]
Gypsum	36	7.5	[35]
Natural Jordanian Tripoli	16.6	8.0	[36]

3.10.1 pseudo-first-order kinetics

The nonlinear form of the pseudo-first equation is obtained according to following equations [32].

$$\frac{dq_t}{dt} = k_1(q_e - q_t) \tag{5}$$

$$\log(q_e - q_t) = \log(q_e) - \frac{k_1}{2.303}t \tag{6}$$

In this regard, q_e and q_t are the amount of adsorbed material in terms of mg/g in equilibrium and at time t, respectively, k_1 is the rate constant in terms of 1/min (Fig. 10).

The correlation coefficient for pseudo-first-order kinetics was 0.971.

Adsorption kinetic equations are used to investigate the mechanisms that control the adsorption process such as diffusion, adsorption, intramolecular adsorption, and chemical adsorption. If the adsorption control factor is the diffusion in the boundary layer, the adsorption kinetics usually follows a pseudo-first-order model. Thus, the change of adsorption rate over time are proportional to the number of unoccupied sites at the adsorbent surface [33].

3.10.2 Pseudo-second order kinetic model

In the pseudo-second-order model, it is assumed that chemical adsorption controls the adsorption phenomenon and the rate of occupation of adsorption sites is proportional to the square of the number of inactive sites. If the pseudo-second-order model is applicable, the t/q_t curve will increase as a function of t of a straight line with a correlation coefficient.

$$\frac{dq_t}{dt} = k_2(q_e - q_t)^2 \tag{7}$$

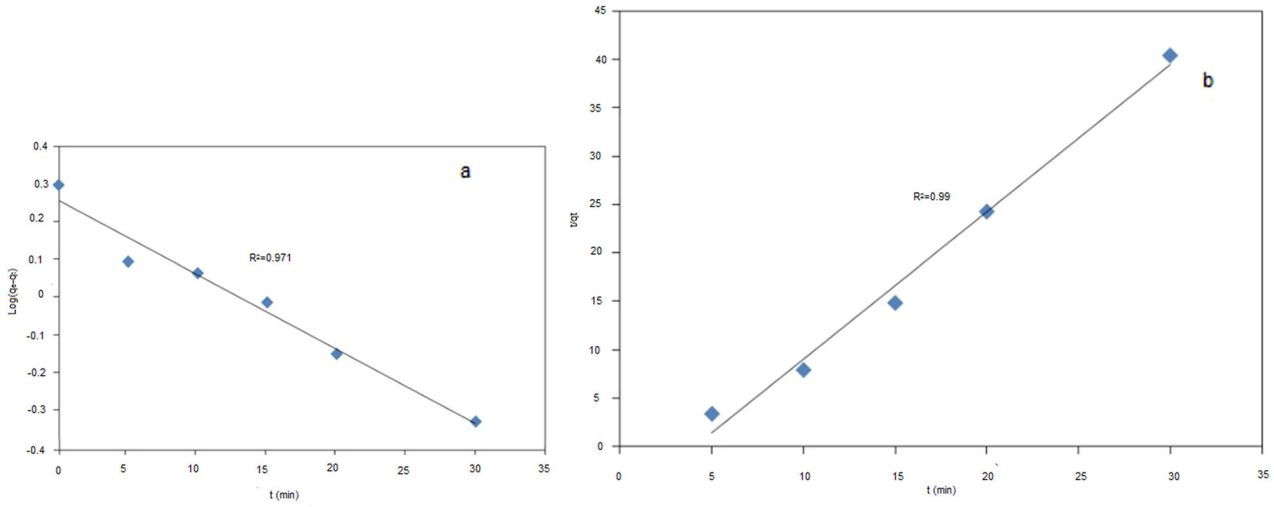

Fig. 10 Adsorption kinetic **a** quasi-first-order equation pattern **b** quasi-second-order equation pattern

$$\frac{t}{q_t} = \frac{1}{k_2 q_e^2} + \frac{1}{q_e} t \tag{8}$$

In this relation, q_e and q_t are the amount of adsorbed material in terms of mg/g, respectively, in equilibrium at time t, and k_2 is the rate constant in terms of g/mg min. Figure 10 shows the results of matching the experimental results to the pseudo-second-order model.

As can be seen, the correlation coefficient for pseudo-first-order kinetics was 0.99. Therefore, the correlation coefficient provides a better fit with the pseudo-second-order model than that of the pseudo-first-order kinetic model for adsorption of methylene blue dye solution on the nanocomposite.

4 Conclusion

Al_2O_3–$ZnAl_2O_4$ nanocomposite was synthesized using sol–gel method and heat treated at 700 °C causes crystallization of $ZnAl_2O_4$ crystals in the composite. The size of $ZnAl_2O_4$ crystals increases with increasing the weight percentage of $ZnAl_2O_4$ in the composite. The average size of crystals in the maximum amount of $ZnAl_2O_4$ in the composite was calculated to be 27 nm by Williamson–Hall method. SEM showed that with increasing the percentage of $ZnAl_2O_4$ in the morphological composite, it changes from sheet to mass. The results of BET test showed the mesoporous nature of the cavities with the specific surface area of the nanocomposite is 70 m^2/g at the maximum value. The highest adsorption efficiency (72%) was obtained by having the initial concentration of methylene blue dye equal to 10 mg/L, the amount of adsorbent (Al_2O_3–70% $ZnAl_2O_4$ nanocomposite) equal to 0.05 g, pH = 8.5. The pseudo-second-order model with a higher correlation coefficient ($R^2 = 0.99$) was the best choice for describing the adsorption behavior of the dye in the system.

Compliance with ethical standards

Conflict of interest The authors declare no competing interests.

Publisher's note Springer Nature remains neutral with regard to jurisdictional claims in published maps and institutional affiliations.

References

1. Sukul G, Balaramakrishna PV (2014) Novel $ZnAl_2O_4$:SiO_2 nanocomposites for high temperature refractory applications. Mater Sci Eng 64:1–6
2. Tzing WS, Tuan WH (1996) The strength of duplex AI_2O_3-$ZnAI_2O_4$ composite. J Mater Sci Lett 15:1395–1396
3. Zhang L, Yana J, Zhou M, Yang Y, Liu YN (2013) Fabrication and photocatalytic properties of spheres-in-spheres ZnO/$ZnAl_2O_4$ composite hollow microspheres. Appl Surf Sci 268:237–245
4. Sommer S, Bøjesen ED, Reardon H, Iversen BB (2020) Atomic scale design of spinel 4. $ZnAl_2O_4$ nanocrystal synthesis. Crys Growth Des 20:1789–1799
5. Dutta K, Das S, Pramanik A (2012) Concomitant synthesis of highly crystalline Zn–Al layered double hydroxide and ZnO: phase interconversion and enhanced photocatalytic activity. J Colloid Interface Sci 366:28–36
6. Stringhini FM, Foletto EL, Sallet D, Bertuol DA, Filho OC, Nascimento CAO (2014) Synthesis of porous zinc aluminate spinel ($ZnAl_2O_4$) by metal-chitosan complexation method. J Alloy Compd 588:305–309
7. Zidouh H, Ait Baih M, El Qacemi N, Mamouni R, Laknifl A, Saffaj N (2019) Wastewater treatment by $ZnAl_2O_4$ ultrafiltration ceramic membrane. Int J Mater Sci 2:99–105
8. Zhaoxia B, Rong Z, Weiping L, Xusheng W, Shulin G, Bo S, Yi S, Zhiguo L, Youdou Z (2003) Synthesis of $ZnAl_2O_4$/Al_2O_3 complex substrates and growth of GaN films. Sci China 46:42–46
9. Foletto EL, Battiston S, Simoes JM, Bassaco MM, Pereira LSF, Flores EMM, Muller EI (2012) Synthesis of $ZnAl_2O_4$ nanoparticles

by different routes and the effect of its pore size on the photocatalytic process. Microporous Mesoporous Mater 163:29–33. 2012
10. Ianos R, Borcanescu S, Lazau R (2014) Large surface area $ZnAl_2O_4$ powders prepared by a modified combustion technique. Chem Eng J 240:260–263. 2014
11. Zhu Z, Li X, Zhao Q, Liu S, Hu X, Chen G (2011) Facile solution synthesis and characterization of porous cubic-shaped superstructure of $ZnAl_2O_4$. Mater Lett 65:194–197
12. Meena AK (2006) Studies on treatment of contaminated water containing heavy metals in Jaipur and Pali", Ph.D. thesis, University of Rajasthan, India
13. Tao P, Shao M, Song CH, Wu SH, Cheng M, Cui ZH (2014) Preparation of porous and hollow Mn_2O_3 microspheres and their adsorption studies on heavy metal ions from aqueous solutions. J Ind Eng Chem 20:3128–3133
14. Joyner RW (1991) Principles of catalyst development. Adv Mater 3:170–171. 1991
15. Farhadi S, Jahanaram K (2014) $ZnAl_2O_4$@SiO_2 nanocomposite catalyst for the acetylation of alcohols, phenols and amines with acetic anhydride under solvent-free conditions. Chin J Catal 35:368–375
16. Motloung S, Dejene F, Swart H, Ntwaeaborwa O (2011) Sol-gel synthesis and characterization of structural and luminescence properties of $ZnAl_2O_4$ doped with Mn^{2+} powder phosphor. J Mater Sci 46:6981–6987
17. Ramesh S (2013) Sol-gel synthesis and characterization of $Ag_{3(2+x)}Al_xTi_{4-x}O_{11+\delta}$ ($0.0 \le x \le 1.0$) nanoparticles. J Nanosci 2013:1–8
18. Wang SF, Sun GZ, Fang LM, Lei L, Xiang X, Zu XT (2015) A comparative study of $ZnAl_2O_4$ nanoparticles synthesized from different aluminum salts for use as fluorescence materials. Sci Rep. 5:1–12. 2015
19. Sing SW, Everett DH, Haul RAW, Moscou L, Pierotti RA, Rouquerol J, Siemieniewska T (1985) Reporting physisorption data for gas/solid systems, with special reference to the determination of surface area and porosity. Pure Appl Chem 57:603–619
20. Royer B, Cardoso NF, Lima EC, Vaghetti JCP, Simon NM, Calvete T, Veses RC (2009) Applications of Brazilian-pine fruit shell in natural and carbonized forms as adsorbents to removal of methylene blue from aqueous solutions- kinetic and equilibrium study. J Hazard Mater 164:1213–1222
21. Mahmoud MS, Farah JY, Farrag TE (2013) Enhanced removal of Methylene Blue by electrocoag ulation using iron electrodes. Egypt J Pet 22:211–217
22. Anbia M, Asl Hariri S (2010) "Removal of methylene blue from aqueous solution using nanoporous SBA-3. Desalination 261:61–66
23. Gulnaz O, Sahmurova A, Kama S (2011) Removal of Reactive Red 198 from aqueous solution by *Potamogeton crispus*. Chem Eng J 174:579–585
24. Kushwaha AK, Gupta N, Chattopadhyaya MC (2014) Removal of cationic methylene blue and malachite green dyes from aqueous solution by waste materials of *Daucus carota*. J Saudi Chem Soc 18:200–207
25. Nezam A, Saffar-Teluri A, Hassanzadeh-Tabrizi SA (2016) The high efficiency of Al_2O_3–SiO_2–CuO nanocomposites as an adsorbent: synthesis and dye removal efficiency. Res Chem Intermd 42:4999–5011
26. Ni ZM, Xia SJ, Wang LG, Xing FF, Pan GX (2007) Treatment of methyl orange by calcined layered double hydroxides in aqueous solution: adsorption property and kinetic studies. J Colloid Interface Sci 316:284–29
27. Sujoy KD, Bhowal J, Akhil RD, Guha AK (2006) Adsorption behavior of rhodamine B on *Rhizopus oryzae* biomass. Langmuir 22:7265–7272
28. Delrio A. I, Fernandez J, Molina J, Bonastre J, Cases F (2011) Electrochemical treatment of a synthetic wastewater containing a sulphonated azo dye. Determination of naphthalenesulphonic compounds produced as main by-products. Desalination 273:428–435
29. Motlagh MM, Hassanzadeh-Tabrizi SA, Saffar-Teluri A (2015) Sol–gel synthesis of Mn_2O_3/Al_2O_3/SiO_2 hybrid nanocomposite and application for removal of organic dye. J Sol-Gel Sci Technol 73:9–13
30. Bouzid H, Rabiller-Baudry M (2008) Impact of zeta potential and size of caseins as precursors of fouling deposit on limiting and critical fluxes in spiral ultrafiltration of modified skim milks. J Membr Sci 314:67–75
31. Azizian S (2004) Kinetic models of sorption: a theoritical study. J Colloid Interface Sci 276:47–52
32. Ofomaja AE (2010) Intraparticle diffusion process for lead (II) biosorption onto mansonia wood sawdust. Bioresour Technol 101:5868–5876
33. Wang S, Boyjoo Y, Choueib A (2005) A comparative study of dye removal using fly ash treated by different methods. Chemosphere 60:1401–7
34. Saffar A, Abbastabar Ahangar H, Aghili A, Hassanzadeh-Tabrizi SA, Aminsharei F, Rahimi H, Alikhani Kupai J (2020) Synthesis of the novel $CuAl_2O_4$–Al_2O_3–SiO_2 nanocomposites for the removal of pollutant dye and antibacterial applications. Res Chem Intermed 47:599–612
35. Rauf MA, Shehadeh I, Ahmed A, Al-Zamly A (2009) Removal of methylene blue from aqueous solution by using gypsum as a low cost adsorbent. World Acad Sci Eng Technol 31:604–609
36. Alzaydien AS (2009) Adsorption of methylene blue from aqueous solution onto a low-cost natural Jordanian Tripoli. Am. J Environ Sci 5:197–208